

Structural and superconducting properties of RbOs_2O_6 single crystals

Krzysztof Rogacki,^{1,2,*} Götz Schuck,³ Zbigniew Bukowski,¹ Nikolai D. Zhigadlo,¹ and Janusz Karpinski¹

¹Laboratory for Solid State Physics, ETH Zürich, 8093 Zürich, Switzerland

²Institute of Low Temperature and Structure Research, PAS, 50-950 Wrocław, Poland

³Laboratory for Neutron Scattering, PSI, 5232 Villigen, Switzerland

(Received 14 July 2007; revised manuscript received 15 September 2007; published 18 April 2008)

Single crystals of RbOs_2O_6 have been grown from Rb_2O and Os in sealed quartz ampoules. The crystal structure has been identified at room temperature as cubic with the lattice constant $a=10.1242(12)$ Å. The anisotropy of the tetrahedral and octahedral networks is lower and the displacement parameters of alkali metal atoms are smaller than those for KOs_2O_6 , so the “rattling” of the alkali atoms in RbOs_2O_6 is less pronounced. The superconducting properties of RbOs_2O_6 in the mixed state have been described well within the London approach and the Ginzburg–Landau parameter $\kappa(0)\cong 31$ has been derived from the reversible magnetization. This parameter is field dependent and changes at low temperatures from $\kappa\cong 22$ (low fields) to $\kappa\cong 31$ at H_{c2} . The thermodynamic critical field $H_c(0)=1.3$ kOe and the superconducting gap $2\Delta_0/k_B T_c\cong 3.2$ have been estimated. These results, together with the slightly different $H_{c2}(T)$ dependence obtained for crystals and polycrystalline RbOs_2O_6 , evidently prove that this compound is a weak-coupling BCS-type superconductor close to the dirty limit.

DOI: 10.1103/PhysRevB.77.134514

PACS number(s): 74.70.Dd, 74.25.Op, 61.66.Fn, 81.10.Bk

I. INTRODUCTION

The recent discovery of superconductivity in the β -pyrochlore compound KOs_2O_6 (Ref. 1) has renewed both theoretical and experimental interest in the properties of superconductors with geometrical frustration in a triangular lattice, which may give rise to many interesting phenomena including the “rattling” behavior of atoms in spacious lattice sites.^{2,3} There is strong experimental evidence that superconductivity in KOs_2O_6 is unconventional^{4–6} and possibly related to its noncentrosymmetric structure.⁷ Thus, unconventional pairing has been considered for this compound, which is superconducting at $T_c=9.6$ K and shows an extremely large upper critical field at zero temperature $H_{c2}(0)\approx 300$ kOe.^{5,8} This field is much higher than the paramagnetic limiting field in the BCS approach, $H_p(0)=18.4T_c\approx 180$ kOe, indicative of pairing with the p -wave symmetry; however, an explanation considering s -wave pairing and extremely strong electron-phonon coupling has been proposed as well.^{4,6} The list of superconducting β pyrochlores also includes CsOs_2O_6 and RbOs_2O_6 with $T_c\approx 3$ and 6 K, respectively. For these compounds, which until now have been available in a polycrystalline form only, no inversion symmetry breaking has been found⁹ and a rather conventional weak-coupling^{10–12} or intermediate-coupling¹³ BCS-type superconductivity has been reported. However, for RbOs_2O_6 , a more unusual mechanism of superconductivity has been also considered on the basis of specific heat measurements.^{14,15} Since the thermodynamic properties of the β -pyrochlore superconductors are sensitive to impurities and other inhomogeneities¹⁶ and since, very often, the polycrystalline RbOs_2O_6 contains an amount of trace impurities,^{13,15,17–19} studies of high quality single crystals are important to avoid possible ambiguity for obtained results. Moreover, it was pointed out that for polycrystalline pyrochlore materials, some normal-state and superconducting properties cannot be estimated properly because of an uncertainty from the grain-surface effects.¹⁹

The crystal structure of α -pyrochlore $A_2B_2O_6O'$ is cubic, where atoms from each A and B sites constitute a corner sharing three-dimensional tetrahedral network called the pyrochlore network. For the α pyrochlore with $Fd\bar{3}m$ symmetry, all tetrahedra of each sublattice are crystallographic equivalent. This is not the case for the low temperature phase of superconducting $\text{Cd}_2\text{Re}_2\text{O}_7$, where two different Re and Cd tetrahedra are present (breathing-mode-like behavior), so the breaking of the inversion symmetry is observed.²⁰ The β -pyrochlore $\square B_2O_6A'$ ($B=\text{Os}$; $A'=\text{K}, \text{Rb}$; \square represents a vacancy) structure can be described as a modified α -pyrochlore structure where β -pyrochlore A' atoms occupy the O' sites and the α -pyrochlore A sites are empty. Recently, the crystal structure of RbOs_2O_6 and KOs_2O_6 was described within the $Fd\bar{3}m$ symmetry.^{9,21} However, for high quality KOs_2O_6 single crystals, the noncentrosymmetric $F\bar{4}3m$ space group was also proposed in order to explain the additional Bragg reflections, which violated the $Fd\bar{3}m$ symmetry.⁷

In this paper, we examine the structural and superconducting properties of high quality RbOs_2O_6 single crystals. We show that the centrosymmetric β -pyrochlore structure is violated at room temperature; however, the atomic shifts from the centrosymmetric positions are lower than those reported for KOs_2O_6 . The superconducting properties of RbOs_2O_6 crystals are rather conventional and differ much from those observed for KOs_2O_6 . We have considered the possible reason for the observed differences and found that the rattling intensity of the alkali metal atoms seems to be the most important parameter that controls the superconducting properties of the β pyrochlores. Such a statement is recently beginning to emerge from both experimental and theoretical studies, as implied in Refs. 3, 6, 19, and 22.

II. EXPERIMENT

Single crystals of RbOs_2O_6 have been grown from stoichiometric amounts of Os metal (Alfa Aesar, 99.9%) and

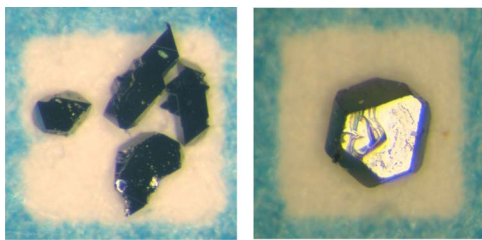


FIG. 1. (Color online) Single crystals of RbOs_2O_6 grown in quartz ampoules. The edge of each individual picture is about 1 mm.

Rb_2O (Aldrich). The components were thoroughly mixed and pressed into pellets in a dry box and sealed in an evacuated quartz ampoule together with an appropriate amount of Ag_2O (Aldrich, 99%) as a source of oxygen. The ampoule was placed in a preheated furnace at 600°C , kept for 10–15 h then slowly ($5^\circ\text{C}/\text{h}$) cooled to 400°C , and, finally, fast cooled to room temperature. Because of the strong reaction of the pellets with the quartz, alumina crucibles have been used to isolate the pellets from the ampoule walls. Single crystals of RbOs_2O_6 were found on the walls of the alumina crucible indicating that the crystals grew from a gas phase. The crystals have shapes of flattened octahedra and sizes up to $0.3 \times 0.4 \times 0.4 \text{ mm}^3$ (Fig. 1). Energy dispersive x-ray analysis (EDX) indicate slight Rb deficiency but this result should be taken with caution because of the strong overlapping of Os and Rb lines in the EDX spectrum.

The structural properties of the RbOs_2O_6 single crystals have been investigated at room temperature with an x-ray single-crystal diffractometer [Siemens SMART charge coupled device (CCD) system] using graphite-monochromated $\text{Mo } K\alpha$ radiation.²³ 1818 frames were measured with an exposure time of 10 s per frame and $\Delta\Omega = 0.3^\circ$. The cubic unit cell parameter $a = 10.1242(12) \text{ \AA}$ was refined from 4094 reflections. The three-dimensional data were reduced and corrected for Lorentz, polarization, and background effects using SAINT and for absorption and the $\lambda/2$ contamination using SADABS.^{23,24} In order to verify the correction for the $\lambda/2$ contamination, a similar procedure was applied for an MgB_2 single-crystal data set obtained with the same diffractometer and the results have confirmed the reliability of our correction. The structure was solved by direct methods using SHELXS-97.²⁵ The full matrix least-squares refinement on F^2 was achieved with SHELXL-97.^{25,26}

The superconducting properties of the RbOs_2O_6 single crystals have been investigated by measurements of the magnetic moment m as a function of temperature and magnetic field employing a Quantum Design superconducting quantum interference device magnetometer (MPMS-5) equipped with a 5 T magnet. Individual crystals with a mass of about $40 \mu\text{g}$ as well as a set of two crystals with a mass of $82 \mu\text{g}$ were studied to obtain quantitative results. The magnetic moment m was measured at constant field upon heating from the zero-field-cooled (ZFC) state (ZFC mode) and upon cooling [Add-cooled(FC mode)], or at constant temperature with increasing and decreasing field. The temperature sweep was about $0.2 \text{ K}/\text{min}$ resulting in an accuracy with which m is

TABLE I. Crystallographic and structure refinement parameters of β -pyrochlore RbOs_2O_6 at room temperature. The refinement was performed with Siemens SMART CCD diffractometer data (graphite-monochromated $\text{Mo } K\alpha$ radiation, $\lambda = 0.71073 \text{ \AA}$). The edge length was 0.08 mm . The calculated material density $\rho = 7.193 \text{ g}/\text{cm}^3$ and the calculated absorption coefficient $\mu = 58.200 \text{ mm}^{-1}$.

Space group (crystal system)	$F\bar{4}3m$ (cubic)
Unit cell a (\AA); Z	10.1242(12); 8
Volume (\AA^3)	1037.7(2)
θ range (deg)	3.49–33.79
$h_{\min}; k_{\min}; l_{\min}$	–15; –15; –15
$h_{\max}; k_{\max}; l_{\max}$	15; 15; 15
Extinction coefficient	0.003 21(13)
Flack parameter	0.61(12)
Total reflections measured	4053
Symmetry-equivalent reflection; variables	249; 16
$R_{\text{int}}; R_{\text{sig}}$	0.0571; 0.0234
$R[F^2 > 2\sigma(F^2)]; wR(F^2)$	0.0194; 0.0371
S (observed data); $(\Delta/\sigma)_{\text{max}}$	1.445; 0.000
Largest $\Delta\rho$ (x, y, z), max; min ($e/\text{\AA}^3$)	2.997; –1.035

measured to be better than $1 \times 10^{-6} \text{ emu}$, also in high magnetic fields, for an option where results of three scans were averaged to obtain each individual experimental point.

III. CRYSTAL STRUCTURE

Low-intensity x-ray reflections forbidden in the β -pyrochlore structure with the centrosymmetric space group $Fd\bar{3}m$ have been observed for our RbOs_2O_6 crystals at room temperature. These reflections were present despite the fact that the correction for the $\lambda/2$ contamination has been performed. After averaging symmetry-equivalent reflections, nine reflections inconsistent with d -glide symmetry ($0kl:k+l \neq 4n$, e.g., 024) and four reflections inconsistent with 4_1 screw axis ($00l:l \neq 4n$, e.g., 002) of $Fd\bar{3}m$ persist [$I > 3\sigma(I)$]. This clearly indicates that the previously proposed symmetry of the $Fd\bar{3}m$ space group is broken. No indication for a tetragonal splitting and no reflections which break the F centering (h, k, l not all even or not all odd) have been found. The observed symmetry lowering results in the cubic noncentrosymmetric space group $F\bar{4}3m$. The Os atom has been located at the position 16e using the direct method. The positions of the other atoms were derived from results obtained for KO_2O_6 .⁷ The high quality of RbOs_2O_6 crystals allowed us to refine the anisotropic displacement parameters (ADPs) for all atoms. As a result, the final refinement yielded a residual of $R_1 = 0.0194$. Results of the x-ray measurements and refined atomic parameters are given in Tables I and II. Selected interatomic distances and bond angles are given in Table III. Some structural details are shown in Fig. 2.

The Rb1-O2 bond length is shorter than the Rb2-O1 bond length (the Rb-O bond length difference $\Delta_{\text{Rb-O}} = 0.0314 \text{ \AA}$)

TABLE II. Atomic coordinates, anisotropic (U_{ij}) and isotropic (U_{iso}) displacement parameters (in \AA^2) for RbOs_2O_6 and, to compare, U_{iso} for KOs_2O_6 (Ref. 7). The results were obtained at room temperature with the noncentrosymmetric space group $F\bar{4}3m$.

RbOs_2O_6	Os	Rb1	Rb2	O1	O2
Site	16e	4c	4b	24f	24g
X	0.875 79(5)	$\frac{1}{4}$	$\frac{1}{2}$	0.1899(12)	0.557(2)
Y	X	$\frac{1}{4}$	$\frac{1}{2}$	0	$\frac{1}{4}$
Z	X	$\frac{1}{4}$	$\frac{1}{2}$	0	$\frac{1}{4}$
U_{11}	0.009 3(2)	0.0357(14)	0.0431(16)	0.001(4)	0.036(7)
U_{22}	0.009 3(2)	0.0357(14)	0.0431(16)	0.013(3)	0.019(4)
U_{33}	0.009 3(2)	0.0357(14)	0.0431(16)	0.013(3)	0.019(4)
U_{23}	0.000 66(6)	0	0	0.004(4)	0.014(4)
U_{13}	-0.000 66(6)	0	0	0	0
U_{12}	0.000 66(6)	0	0	0	0
U_{iso}	0.009 3(2)	0.0357(14)	0.0431(16)	0.0087(17)	0.025(2)
KOs_2O_6	Os	K1	K2	O1	O2
U_{iso}	0.0005(1)	0.063(5)	0.062(4)	0.005(1)	0.005(1)

and, consequently, the Os-O2 bond length is longer than Os-O1 ($\Delta_{\text{Os-O}}=0.026 \text{ \AA}$). This leads to anisotropic alkali metal channels (Fig. 2 and Table III), where Rb2 atoms have more space to move, so they oscillate with a larger amplitude. The anisotropy of the alkali metal channels is also reflected in the refined ADPs of the Rb and O atoms. The ADPs of Rb2 and O2 are much larger than the ADPs of Rb1 and O1. Moreover, the O2 displacement ellipsoid is elongated toward the Rb1 atom, whereas the O1 displacement ellipsoid is not oriented in the consistently similar way, i.e., this ellipsoid does not point to the Rb2 atom. Summarizing, the lowering of symmetry from $Fd\bar{3}m$ to $F\bar{4}3m$ results in the bond length differences in both OsO_6 and O_6 octahedral networks ($\Delta_{\text{Os-O}}=0.026 \text{ \AA}$, $\Delta_{\text{O-O}}=0.041 \text{ \AA}$) leading to a breathing-mode-like behavior. Refined ADPs, Δ , and U_{iso} show that the anisotropy of the alkali metal channels and the rattling of the alkali metal atoms obtained for RbOs_2O_6 are much lower than those for KOs_2O_6 (see Tables II and III). This may explain the exceptionally different superconducting properties of the KOs_2O_6 compound if compared to the properties of the other members of the β -pyrochlore family.

As mentioned in the Introduction, the crystal structure of RbOs_2O_6 has been previously described by Galati *et al.*⁹ within the centrosymmetric space group $Fd\bar{3}m$. This result has been obtained from the powder neutron diffraction (PND) experiments, where no Bragg reflections forbidden for the centrosymmetric structure have been observed. Considering the resolution of the PND measurements, we may speculate that the low-intensity reflections, which violate the $Fd\bar{3}m$ symmetry, are hidden in the background. The background may be additionally enhanced for polycrystalline samples where some amount of trace impurities is usually present.^{13,15,17-19} Consequently, the evidence for the inversion symmetry breaking in the β -pyrochlore compounds may be observed for very pure material only, particularly in the single-crystal form.

TABLE III. Selected interatomic distances (\AA) and bond angles (deg) for RbOs_2O_6 and KOs_2O_6 (Ref. 7) obtained within the noncentrosymmetric space group $F\bar{4}3m$. The length difference Δ caused by lowering of the symmetry from $Fd\bar{3}m$ (ideal β -pyrochlore structure) to $F\bar{4}3m$ is defined as $\Delta = (\text{maximum length}) - (\text{minimum length})$. The numbers in square brackets indicate bond multiplicities.

β pyrochlore	RbOs_2O_6	Δ (\AA)	KOs_2O_6	Δ (\AA)
Osmium environment				
Os-O1	³ 1.899(4)	0.026	1.920(5)	0.014
Os-O2	³ 1.925(7)		1.906(4)	
O1-Os-O1	91.5(5)		94.2(5)	
O1-Os-O2	88.3(2)		87.8(3)	
O2-Os-O2	91.9(8)		90.1(5)	
O1-Os-O2	179.7(9)		177.0(6)	
Os-O1-Os	139.0(7)		137.7(3)	
Os-O2-Os	138.4(11)		138.9(6)	
Tetrahedral network				
Os-Os	⁴ 3.5568(8)	0.0453	3.548(4)	0.044
Os-Os	⁴ 3.6021(8)		3.592(5)	
Alkali metal (A') environment				
$A'1$ -O2	⁸ 3.1081(4)	0.0314	3.141(13)	0.082
$A'2$ -O1	⁸ 3.1395(4)		3.059(13)	
$A'1$ - $A'2$	⁴ 4.3839(3)		4.3720(4)	
Octahedral network: OsO_6 octahedra				
O1-O2	⁶ 2.666(5)		2.653(4)	
Octahedral network: O_6 octahedra				
O1-O1	⁸ 2.719(12)	0.041	2.819(5)	0.124
O2-O2	⁸ 2.76(2)		2.695(4)	

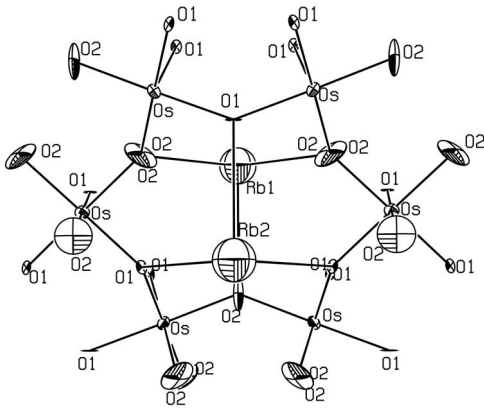


FIG. 2. Structural details of RbOs_2O_6 at room temperature ($F\bar{4}3m$ space group) showing the anisotropic nature of the rubidium channels (structure projected along the $[-110]$ direction). Interatomic distances Rb1-O2 and Rb2-O1 are shorter (3.1081 \AA) and longer (3.1395 \AA), respectively, compared to the β -pyrochlore structure with $\bar{3}m$ symmetry [$\text{Rb-O}=3.125(7) \text{ \AA}$]. The O2 displacement ellipsoid is elongated toward the Rb1 atom whereas the O1 displacement ellipsoid does not point to the Rb2 atom. The displacement ellipsoids are drawn at the 50% probability level.

IV. SUPERCONDUCTING PROPERTIES

The superconducting transition temperature T_c was determined from changes of the magnetic moment m with temperature at constant field. As an example, Figs. 3 and 4 show $m(T)$ results for two RbOs_2O_6 single crystals with similar $T_c \approx 6.2 \text{ K}$. The transition temperature T_c and the transition onset temperature T_{co} were defined as illustrated in Fig. 3. The transition temperature difference, $\Delta T_c = T_{co} - T_c$, was determined and identified with crystal quality. This temperature difference varied from 0.05 to 0.15 K, depending on a batch. For high quality crystals, $\Delta T_c \approx 0.05 \text{ K}$ is roughly field independent at low fields and drops below the resolution of $\Delta T_c \approx 0.02 \text{ K}$ at $H \geq 4 \text{ kOe}$. This seems to confirm a pure bulk transition (no surface effects) to the superconducting

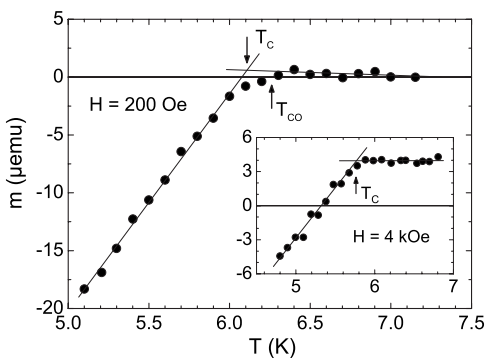


FIG. 3. Magnetic moment vs temperature at constant fields $H=0.2 \text{ kOe}$ and 4 kOe (inset) for the RbOs_2O_6 single crystal with $T_c=6.25 \text{ K}$ at 5 Oe . The superconducting transition temperature T_c and the transition onset temperature T_{co} are marked by arrows. For $H=4 \text{ kOe}$, $T_{co} \approx T_c=5.76 \text{ K}$, indicative of a bulk transition to the superconducting state.

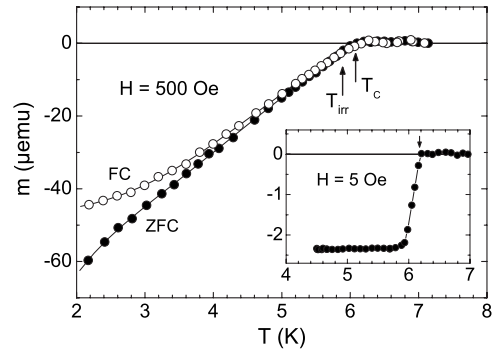


FIG. 4. Magnetic moment vs temperature at constant fields $H=500 \text{ Oe}$ and 5 Oe (inset) for the RbOs_2O_6 single crystal with $T_c=6.18 \text{ K}$ at 5 Oe . The results are obtained upon heating from the ZFC state and upon cooling (FC). The superconducting transition temperature T_c and the irreversibility temperature T_{irr} are marked by arrows. The beginning of the irreversible $m(T)$ properties at T_{irr} is not visible in this scale.

state at T_c . The presence of T_{co} at low fields can be explained as a result of inhomogeneous field distribution around the crystal due to a large demagnetizing effect expected for the octahedral-shaped crystal. Thus, ΔT_c should increase when the quality of the crystal surface lowers.

In Fig. 4, we show the magnetic moment of the RbOs_2O_6 single crystal measured with increasing (ZFC mode) and decreasing (FC mode) temperature at a field of 500 Oe . A sharp transition to the superconducting state, observed at $T_c = 6.18 \text{ K}$ in 5 Oe (see inset), broadens significantly with increasing field and extends to the lowest available temperatures for $H \geq 200 \text{ Oe}$. This indicates weak pinning properties and, consequently, a low irreversibility field H_{irr} even at low temperatures. For example, at a temperature of 3.4 K , the upper critical field $H_{c2}=28.5 \text{ kOe}$, however, H_{irr} is equal only to about 2 kOe for the critical current criterion $j_c \approx 6 \text{ A/cm}^2$, which corresponds to the magnetic moment resolution $\Delta m \approx 5 \times 10^{-7} \text{ emu}$. The extremely low pinning, and thus H_{irr} , seems to be a more general feature of the β -pyrochlore compounds, as analogous weak pinning properties have been recently reported for KOs_2O_6 crystals.⁷

Results of the magnetic moment measurements similar to those presented in Figs. 3 and 4 have been performed at constant fields up to 50 kOe to obtain the temperature dependence of the upper critical field $H_{c2}(T)$. In Fig. 5, we show the $H_{c2}-T$ phase diagram for the RbOs_2O_6 crystal with $T_c = 6.18 \text{ K}$ at 5 Oe (see the inset of Fig. 4). Special attention has been paid in determining $H_{c2}(T)$ in the vicinity of T_c , resulting in the real initial slope $(-dH_{c2}/dT)_{T_c} = 11.0 \text{ kOe/K}$. This value is slightly lower than the 12 kOe/K reported for polycrystalline samples.¹⁸ The notable increase of the initial slope of $H_{c2}(T)$ observed for polycrystalline RbOs_2O_6 can be explained as a result of the enhanced scattering of quasiparticles due to structural imperfections. This may suggest that the RbOs_2O_6 superconductor is close to the dirty limit. In the inset of Fig. 5, some details of the $H_{c2}(T)$ dependence are shown near T_c . The linear extrapolation of $H_{c2}(T)$ to $H_{c2}=0$ results in $T_c=6.13 \text{ K}$, which is a slightly lower temperature than $T_c=6.18 \text{ K}$ obtained

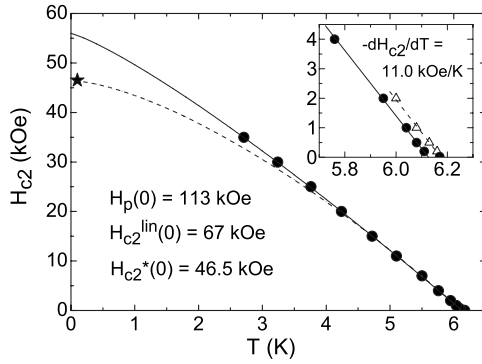


FIG. 5. Upper critical field H_{c2} extracted from the magnetization measurements (circles) for the RbOs_2O_6 single crystal with a bulk transition temperature $T_c=6.13$ K. The solid line is the power law fit $H_{c2}(T)=H_{c2}(0)[1-(T/T_c)^n]$ with an exponent $n=1.2$ and $H_{c2}(0)=56$ kOe. The dashed line is the fit with $n=1.5$ and $H_{c2}^*(0)=46.5$ kOe (star), where $H_{c2}^*(0)$ is the GLAG orbital limiting field in the dirty limit. The inset shows the initial $H_{c2}(T)$ dependence derived with the bulk (circles) and the onset (triangles) transition temperatures. The BCS Pauli limiting field $H_p(0)=113$ kOe is much higher than $H_{c2}^{lin}(0)=67$ kOe obtained from a linear extrapolation of the initial $H_{c2}(T)$ dependence.

from the $m(T)$ measurements performed at $H=5$ Oe. The same $T_c=6.18$ K can be found by the linear extrapolation of the $H_{c2}(T)$ dependence obtained for the transition onset temperature T_{co} (see the inset of Fig. 5). This shows that for our single crystals, the possible surface effects can notably influence the superconducting properties only at low fields. For fields higher than about 100 Oe, the bulk transition to the superconducting state is clearly marked at T_c .

The orbital upper critical field at zero temperature, $H_{c2}^*(0)$, can be obtained in the frame of the Ginzburg–Landau–Abrikosov–Gor’kov (GLAG) theory in the dirty limit from the formula $H_{c2}^*(0)=-0.69(dH_{c2}/dT)_T T_c$.²⁷ Thus, $H_{c2}^*(0)=46.5$ kOe has been calculated for the RbOs_2O_6 crystals with $T_c=6.13$ K. This value has been obtained with the assumption that the spin-orbit scattering parameter $\lambda_{so}=\infty$; thus, the superconducting pairs are broken due to the orbital effects only. The Pauli paramagnetic limiting field in the BCS Clogston approach is $H_p(0)=18.4 T_c \cong 113$ kOe and, consequently, the Maki parameter $\alpha_M=\sqrt{2}H_{c2}^*(0)/H_p(0) \cong 0.58$.^{28,29} This suggests that the spin contribution to the pair-breaking effect is weak and cannot influence H_{c2} significantly.^{27,29,30} In consequence, we assume that $H_{c2}(0) \approx H_{c2}^*(0)=46.5$ kOe and then the simple empirical formula $H_{c2}(T)=H_{c2}(0)[1-(T/T_c)^n]$ with $n=1.5$ is used to obtain the best fitting to the experimental data, as shown in Fig. 5. However, for fields higher than 25 kOe, the calculated curve differs from the experimental data evidently. A similar deviation to higher values of the experimental $H_{c2}(T)$ from the GLAG formula has been recently reported for polycrystalline RbOs_2O_6 .¹⁸ For this material, extrapolated $H_{c2}(0)=56$ kOe has been obtained from resistivity measurements performed down to 1 K.¹⁶ For our single crystals, the best fitting of the empirical formula $H_{c2}(T)=H_{c2}(0)[1-(T/T_c)^n]$ to the experimental points has been found for $H_{c2}(0)=56$ kOe and $n=1.2$, exactly as for polycrystalline samples. Note that even a

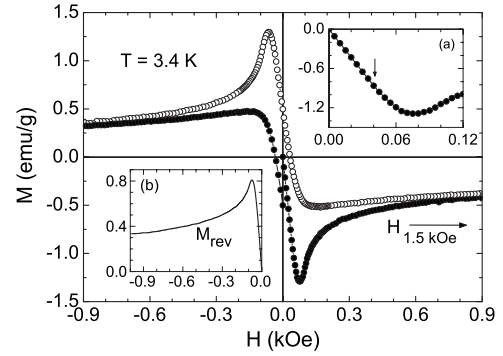


FIG. 6. Magnetization loop $M(H)$ obtained at 3.4 K for H swept from zero to 1.5 kOe (closed circles), then to -1.5 kOe (open circles), and then back to zero (closed circles). Inset (a) shows the virgin curve of the $M(H)$ loop, which was used to determine the first penetration field H_{fp} . The first deviation from the linear part of the virgin curve is marked by an arrow. Inset (b) shows the reversible magnetization M_{rev} calculated from the $M(H)$ half-loop (see text).

linear extrapolation of $H_{c2}(T)$ from T_c , where $-dH_{c2}/dT=11.0$ kOe/K, to $T=0$ K results in $H_{c2}^{lin}(0) \cong 67$ kOe, which is a much lower value than $H_p(0) \cong 113$ kOe. Thus, we can conclude that RbOs_2O_6 is in the orbital limit, much away from the paramagnetic limit, and the extrapolated $H_{c2}(0)=56$ kOe can be used to derive the Ginzburg–Landau (GL) coherence length at zero temperature, $\xi(0)=[\Phi_o/2\pi H_{c2}(0)]^{1/2} \cong 7.7$ nm, where Φ_o is the magnetic flux quantum. Then, the GL parameter can be estimated as $\kappa=\lambda(0)/\xi(0) \cong 32$, with the GL penetration depth $\lambda(0) \cong 250$ nm obtained in the recent muon-spin-rotation experiments for polycrystalline RbOs_2O_6 .^{10,11} This relatively large κ enables us to evaluate the lower critical field by using the BCS formula $H_{c1}(0)=\Phi_o \ln \kappa/4\pi\lambda^2 \cong 91$ Oe. This field is only slightly higher than the first penetration field H_{fp} derived from the $m(H)$ measurements, as we will discuss in the next paragraph. A similar $H_{c1}(0)=92$ Oe was obtained for the polycrystalline compound from the specific heat measurements.¹³

Magnetic moment versus field has been measured at constant temperature to examine the reversible magnetization M_{rev} , the first penetration field H_{fp} , and the shielding effect simultaneously for two RbOs_2O_6 crystals with masses of 51 and 31 μg and dimensions of roughly $0.12 \times 0.2 \times 0.3$ and $0.12 \times 0.12 \times 0.3$ mm³, respectively. Figure 6 shows the magnetization loop $M(H)$ obtained at 3.4 K for H swept between 1.5 and -1.5 kOe beginning from zero. This loop is very narrow and signifies weak pinning and low irreversibility field, consistently with the $m(T)$ results. For $T=3.4$ K, this field is $H_{irr} \approx 2$ kOe despite of the much higher $H_{c2}=28.5$ kOe. The beginning of the magnetization loop (virgin curve) is shown in inset (a) of Fig. 6. First deviation from the linear part of the $M(H)$ curve is used to obtain H_{fp} , which is an upper limit of the lower critical field H_{c1} . For $T=3.4$ K, the first deviation is observed at $H=41(\pm 1)$ Oe (see the inset), and after correction for demagnetizing effects, this value results in $H_{fp}=82$ Oe. For correction, we used a demagnetizing factor $N=0.5$ for H perpendicular to the [111] crystallo-

graphic direction of the octahedral-shaped crystals.⁷ For this demagnetizing factor and for the theoretical density of 7.15 g/cm³ for RbOs₂O₆, the superconducting volume fraction $V_s=0.97$ (± 0.03) has been estimated. This confirms full diamagnetism of the crystals, certifying their good quality.

The macroscopic properties of superconductors in the mixed state depend on the internal structure of an individual vortex, which is determined by the GL parameter $\kappa=\lambda/\xi$. Both λ and ξ can be field dependent and thus the theoretical description of the macroscopic properties can become more complicated. For example, the London approach, which is a powerful tool in describing the thermodynamically reversible magnetization, has to be modified to fit the experimental data well, as shown for several high- κ superconductors.³¹ Hao *et al.* proposed a model based on a variational method, which resulted in a precise description of the reversible magnetization and in the determination of the thermodynamic critical field H_c and κ as fitting parameters.³² Recently, $M_{rev}(H)$ curves have been used to derive the GL parameters directly from the GL theory by applying the two-band model³³ and the 2-order-parameter theory³⁴ with respect to MgB₂ and YBa₂Cu₃O₇, respectively.

A general expression for $M_{rev}(H)$ curves for type-II superconductors has been proposed by Brandt for both triangular and square flux-line lattices.³⁵ This expression, which was achieved within the GL theory, has been postulated to be valid for the entire range of applied fields $H_{c1} \leq H \leq H_{c2}$. Application of this and other models to analyze the $M_{rev}(H)$ data obtained for our RbOs₂O₆ and KOs₂O₆ single crystals is restricted due to the large demagnetizing factor of these octahedral-shaped samples. So, we explain our results with caution, being aware that using more developed models or more detailed analyses may result in the misinterpretation of the experimental findings.³⁶ Additionally, as shown in many experiments, at low fields, the irreversibility is dominated by a geometrical barrier which renders the determination of the reversible part of the magnetization difficult. However, for fields larger than a few H_{fp} , where H_{fp} is the first penetration field, the irreversibility is attributed mainly to the bulk pinning and the geometrical barrier effect can be neglected. H_{fp} has been estimated to be about 82 and 95 Oe for RbOs₂O₆ (this work) and KOs₂O₆ (Ref. 7) crystals, respectively. Thus, the reversible magnetization is considered only for $H > 200$ Oe $> 2H_{fp}$.

Magnetization loops similar to those shown in Fig. 6 have been used to derive the reversible magnetization curves $M_{rev}(H)$, defined as the average between ascending and descending branches of the magnetization loop. Figure 6 (inset) shows the $M_{rev}(H)$ curve at 3.4 K for the RbOs₂O₆ crystal for the negative-field side of the $M(H)$ loop. A similar $M_{rev}(H)$ curve can be obtained for the positive-field side of the loop if the half-loop instead of the virgin curve (shown in the figure) is considered. This positive-field $M_{rev}(H)$ curve is taken for further analyses and plotted in a semilogarithmic scale in Fig. 7, together with results obtained for KOs₂O₆ crystals. For RbOs₂O₆, a linear $M_{rev}(H)$ dependence is observed in the field range 0.2 kOe $< H < 1.5$ kOe, while for KOs₂O₆, no linear dependence is found at any temperature and field studied. In the intermediate field range (London regime), the reversible magnetization, which is entirely de-

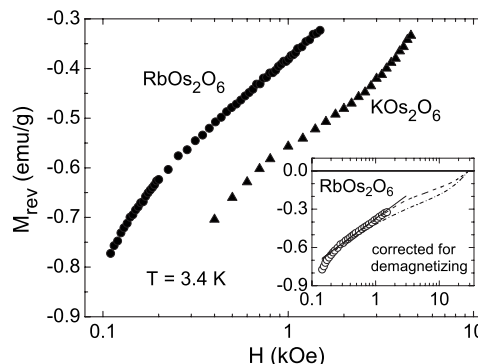


FIG. 7. Reversible magnetization as a function of an applied field for RbOs₂O₆ and KOs₂O₆ single crystals. The data for KOs₂O₆ are shifted with +0.1 emu/g for convenience. The inset shows the experimental $M_{rev}(H)$ data (circles) corrected for demagnetizing effects (see text). The experimental data are compared to the results calculated with Eq. (1) for $\kappa(H)=\text{const}=22.2$ (solid line) and with Eq. (2) for the same κ (dot-dashed line) and for κ being field dependent (dashed line). The dashed line has been obtained for κ changing gradually from 22.2 ($H \sim 0.2$ kOe) to 26.4 ($H \geq 13$ kOe).

finied by $h=H/H_{c2}$ and $\kappa=\lambda/\xi$, is expected to vary linearly with $\ln H$:³⁵

$$4\pi M_{rev} = (-H_{c2}/4\kappa^2)\ln(0.358/h), \quad (1)$$

where M_{rev} is in emu/cm³ and H_{c2} in Oe. According to the calculation of Brandt,^{35,37} the basic requirement to observe a linear M on $\ln H$ dependence is $H < 0.1H_{c2}$. At low temperatures ($T < 0.5T_c$), H_{c2} for RbOs₂O₆ and KOs₂O₆ is higher than 30 and 100 kOe, respectively. Thus, the $M_{rev}(H)$ curves, which were obtained at fields up to 1.5 and 5 kOe for RbOs₂O₆ and KOs₂O₆, respectively, can be used to calculate the GL parameter κ with formula (1). For $T=3.4$ K and $H=0.5$ kOe (see Fig. 7), a volume magnetization $M_{rev}=-3.47$ emu/cm³ is obtained with a crystal density $\rho=7.15$ g/cm³. For $T=3.4$ K, H_{c2} is equal to 28.5 kOe (see Fig. 5) and, consequently, the GL parameter $\kappa=22.2$ is calculated. For fields $H \geq 0.5$ kOe, the correction for demagnetizing effects ($N=0.5$), $H_{cor}=H-N4\pi M$, results in an increase of H of less than 5% and in a decrease of κ of less than 1%, so we neglect this correction in most aspects of further consideration.

The linear $M_{rev}(\ln H)$ dependence, which is observed for RbOs₂O₆ crystals, shows that κ is field independent at low temperatures and fields from 0.25 to at least 2 kOe. Thus, first, we assume that $\kappa(H)=\text{const}$ in the entire field range ($H \leq H_{c2}$) and calculate $M_{rev}(H)$ from the interpolation formula obtained by Brandt:³⁵

$$4\pi M_{rev} = (-H_{c2}/4\kappa^2)\ln\{1 + [(1-h)/h](0.357 + 2.890h - 1.581h^2)\}. \quad (2)$$

The calculated $M_{rev}(H)$ is shown in the inset of Fig. 7, revealing a rather poor fitting to the experimental results. For better fitting, κ is required to be field dependent and to change gradually from 22.2 at low fields to 26.4 at

$H \geq 13$ kOe. Assuming that κ is roughly proportional to H , we can obtain the extrapolated $\kappa(H_{c2}) \approx 31$ at 3.4 K, where $H_{c2} = 28.5$ kOe. This κ , which is expected to be temperature independent or weakly dependent at $T < 0.5T_c$, is very close to $\kappa(0) \approx 32$ derived from $H_{c2}(0)$, as described in the paragraph devoted to the GLAG theory. This may prove the applicability of the standard theories and points to the classical behavior of the RbOs_2O_6 superconductor. A similar $\kappa(0) = 34$ was obtained for the polycrystalline compound from the specific heat measurements.¹³

Now, we can estimate the thermodynamic critical field $H_c(0) = H_{c2}(0) / \sqrt{2\kappa} \approx 1.3$ kOe, with the GL parameter $\kappa = 31$ and $H_{c2}(0) = 56$ kOe, which is a value obtained from the extrapolation of the $H_{c2}(T)$ experimental results (see Fig. 5). The penetration depth λ is related to H_c and κ by $\sqrt{2}H_c = \kappa\Phi_0 / 2\pi\lambda^2$, with which $\lambda_0 = \lambda(0) \approx 240$ nm is calculated. This result is in excellent agreement with the magnetization and muon-spin-rotation (μSR) measurements, where $\lambda_0 \approx 230$ nm was found for polycrystalline material.¹⁰ Later μSR experiments showed that λ_0 ranged from 250 to 300 nm and was almost magnetic field independent at low temperatures.¹¹ Thus, using $\lambda_0 \approx 240$ nm and $\kappa = 31$, which are the values obtained by us from the analysis of the $M_{rev}(H)$ curves, the GL coherence length is estimated to be $\xi_0 = \xi(0) = \lambda_0 / \kappa \approx 7.7$ nm. This is in excellent agreement with ξ_0 derived from the $H_{c2}(T)$ results and is only slightly higher than 7.4 nm obtained for a polycrystalline compound.^{13,18}

Still considering the $M_{rev}(H)$ curves for RbOs_2O_6 crystals (see Fig. 7), we would like to remind that the logarithmic derivative $dM_{rev}/d\ln H$ is field independent in the field range from 0.25 to about 2 kOe. This derivative is expected to be proportional to the superfluid density, which is inversely proportional to the penetration depth. Thus, the $M_{rev}(H)$ behavior can be described well in the London regime and the RbOs_2O_6 compound appears to be a conventional superconductor. Note that for KOs_2O_6 crystals, no clear linear dependence of M_{rev} vs $\ln H$ can be found, so λ seems to be field dependent and the $M_{rev}(H)$ theoretical curve may fit the experimental data only in a very limited field range by using a unique set of κ values. This may emphasize the unusual superconducting properties of the KOs_2O_6 compound in the mixed state including the exceptionally large upper critical field.⁸

Encouraged by the fact that RbOs_2O_6 is revealed as a conventional BCS superconductor, we estimate the energy gap at 0 K, Δ_0 , by using the empirical relation first described by Toxen:³⁸ $[2T_c/H_c(0)][-dH_c(T)/dT]_{T_c} = 2\Delta_0/k_B T_c$, where $dH_c(T)/dT$ is taken at T_c . This relation is usually valid for the weak-coupling regime,³⁹ so we assume it can provide us with reasonable results for RbOs_2O_6 . The $dH_c(T)/dT$ value at T_c was derived from the relation $H_c(T) = H_{c2}(T) / \sqrt{2\kappa}$ with $-dH_{c2}(T)/dT = 11$ kOe/K at $T_c = 6.13$ K (see Fig. 5) and with $\kappa(T_c) = 23$ taken from Ref. 13. For these data, $2\Delta_0/k_B T_c \approx 3.2$ has been obtained, which is close to the weak-coupling BCS value of 3.53 and fits well into the range 3.1–3.6 found for the polycrystalline compound from the μSR measurements.¹¹ This result and all of the above-discussed relevant features definitely confirm that RbOs_2O_6 is a weak-coupling BCS superconductor.

Structural refinements of RbOs_2O_6 crystals reveal a large Rb isotropic displacement parameter at room temperature of

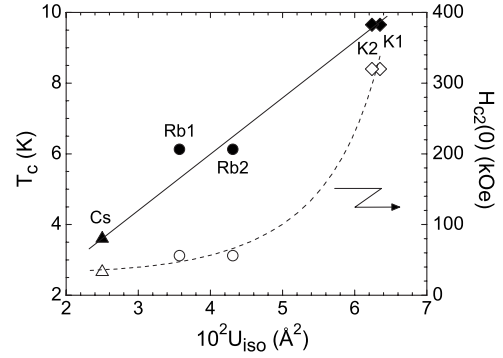


FIG. 8. Superconducting transition temperature (closed symbols) and an upper critical field at zero temperature (open symbols) versus U_{iso} at 300 K of the A' atoms of $A'\text{Os}_2\text{O}_6$ for polycrystalline CsOs_2O_6 (triangles) and single crystals of RbOs_2O_6 (circles) and KOs_2O_6 (diamonds). Results for CsOs_2O_6 were taken from Ref. 21. Results for KOs_2O_6 come from our previous work (Ref. 7).

$100U_{iso} = 3.57$ and 4.31 \AA^2 for Rb1 and Rb2, respectively (see Table II), when the refinements are done within the non-centrosymmetric space group $F\bar{4}3m$. These values are close to $100U_{iso} = 3.41 \text{ \AA}^2$ reported for polycrystalline compound when the structure was refined within the centrosymmetric space group $Fd\bar{3}m$.⁹ The observed relatively large U_{iso} shows enhanced rattling of the Rb atom in the $\text{Os}_{12}\text{O}_{18}$ cage compared to the rattling of the Cs atom ($100U_{iso} = 2.5 \text{ \AA}^2$),²¹ as predicted for the $A'\text{Os}_2\text{O}_6$ ($A' = \text{Cs, Rb, K}$) family from the band structure calculations.⁴⁰ These calculations postulate the largest displacement of the alkali atom for the KOs_2O_6 compound, where a substantial instability in the optic mode of the K atom leads to the extensive rattling behavior. This rattling is expected to create highly anharmonic low frequency phonons, which may influence the transport and thermodynamic properties significantly.^{22,40,41} For single crystals, $100U_{iso} \approx 6.3$ and 7.4 \AA^2 were obtained for the K atom when the structure was refined in the space groups $F\bar{4}3m$ (Ref. 7) and $Fd\bar{3}m$ (Ref. 21), respectively.

The large dissimilarity in the rattling intensity of the alkali metal atoms in the β pyrochlores seems to be the main reason (“structural”) for the different superconducting properties observed for $A'\text{Os}_2\text{O}_6$ with $A' = \text{Cs, Rb, and K}$. This has been indicated in the work by Hiroi *et al.*,¹⁹ where systematic variations of the normal-state and superconducting properties have been considered over the Cs-Rb-K series. Figure 8 shows T_c and $H_{c2}(0)$ versus U_{iso} of the A' atoms for polycrystalline CsOs_2O_6 and single crystals of $A'\text{Os}_2\text{O}_6$ ($A' = \text{Rb, K}$). A roughly linear increase of T_c with U_{iso} is observed across the Cs-Rb-K series. For RbOs_2O_6 , the linear $T_c(U_{iso})$ dependence applies better to atoms which occupy the position $A'2$, i.e., the atoms which vibrate with larger amplitude in more spacious channels of the Os-O network. On the other hand, $H_{c2}(0)$ increases with U_{iso} much steeply, revealing that no scaling between T_c and H_{c2} is possible here in the frame of the BCS theory. Since the crystal and electronic structures of $A'\text{Os}_2\text{O}_6$ ($A' = \text{Cs, Rb, K}$) are essentially the same, and since U_{iso} is a measure of the instability of the alkali atom in the tetrahedral interstitial site, the observed

monotonic relationships $U_{iso}-T_c$ and $U_{iso}-H_{c2}$ suggest that the superconducting properties of these compounds depend more on the lattice dynamics than on the electronic structure. This is consistent with the results of the electronic structure investigations, where the different degrees of anharmonicity of the alkali atom across the K-Rb-Cs series is proposed to be responsible for the differences in the physical properties of these pyrochlores.^{3,40} The lattice dynamics can be also responsible for the breaking of the inversion symmetry of the ideal β -pyrochlore structure to reduce the structural frustration predicted to appear for the tetrahedral sublattice of the alkali atoms.³ Note that the noncentrosymmetric structure has been proposed for KOs_2O_6 (Ref. 7) and is considered for RbOs_2O_6 in this work.

V. CONCLUSION

In this paper, we have examined the structural and superconducting properties of the high quality RbOs_2O_6 single crystals, revealing that RbOs_2O_6 is a conventional superconductor despite of a noncentrosymmetric structure refined at room temperature. The anisotropic character of RbOs_2O_6 is less pronounced than that for KOs_2O_6 ; however, additional reflections which violate the $Fd\bar{3}m$ symmetry have been certainly observed and the noncentrosymmetric $F\bar{4}3m$ space group has been chosen for the interpretation of the crystallographic data. The high quality of RbOs_2O_6 crystals allowed us to refine the anisotropic displacement parameters for all atoms. This refinement shows a strong motion (rattling) of the Rb atoms in the framework of OsO_6 octahedra. The Rb atoms rattle in channels, which are anisotropic due to the breathing-mode-like behavior of the octahedral and tetrahedral networks. The lower displacement of the Rb atoms compared with K atoms in $A'\text{Os}_2\text{O}_6$ is in good agreement with band structure calculations where instability and motion anharmonicity of alkali metal atoms increase toward the Cs-

Rb-K series of the β pyrochlores.⁴⁰ The superconducting properties of the RbOs_2O_6 crystals in the mixed state are described well within the London approach revealing that in this compound, the superconductivity is rather conventional. The superconducting gap $2\Delta_o/k_B T_c \cong 3.2$ has been estimated, indicative of the weak-coupling BCS-type pairing. The values of the coherence length, the GL parameter, and the lower and upper critical fields for single crystals and polycrystalline samples are similar, except for a clear difference observed for the initial slope of $H_{c2}(T)$. These results show that RbOs_2O_6 is slightly sensitive to small inhomogeneities and other imperfections, so RbOs_2O_6 seems to be a superconductor close to the dirty limit. For the $A'\text{Os}_2\text{O}_6$ family, both T_c and H_{c2} increase with U_{iso} toward the Cs-Rb-K series, supporting the belief by some that the superconducting properties of the β pyrochlores depend more on the lattice dynamics than on the electronic structure which for all these compounds is very similar.

Note added. Recently, the crystal structure of KOs_2O_6 and RbOs_2O_6 has been studied on our single crystals by Schoenes *et al.*⁴² using the micro-Raman spectroscopy. The results show that the structure is centrosymmetric in both compounds. Thus, the reflections which violate the centrosymmetric structure we observed could be due to the Renninger effect.⁴³ If this is true, no symmetry breaking is present and the structure of KOs_2O_6 and RbOs_2O_6 belongs to the centrosymmetric $Fd\bar{3}m$ space group. To clarify this issue, advanced studies of the crystal structure of these β pyrochlores have been undertaken using synchrotron *x*-ray experiments.

ACKNOWLEDGMENTS

This work was supported by NCCR MaNEP and the National Science Foundation. The SMART CCD measurements were performed at the Laboratory of Inorganic Chemistry, ETH Zürich. We acknowledge fruitful discussions with M. Wörle (Laboratory of Inorganic Chemistry, ETH Zürich).

*Corresponding author; rogacki@int.pan.wroc.pl

¹S. Yonezawa, Y. Muraoka, Y. Matsushita, and Z. Hiroi, *J. Phys.: Condens. Matter* **16**, L9 (2004).

²J. Kuneš and W. E. Pickett, *Physica B* **378-380**, 898 (2006).

³J. Kuneš and W. E. Pickett, *Phys. Rev. B* **74**, 094302 (2006).

⁴Brühwiler, S. M. Kazakov, J. Karpinski, and B. Batlogg, *Phys. Rev. B* **73**, 094518 (2006).

⁵T. Shibauchi, L. Krusin-Elbaum, Y. Kasahara, Y. Shimono, Y. Matsuda, R. D. McDonald, C. H. Mielke, S. Yonezawa, Z. Hiroi, M. Arai, T. Kita, G. Blatter, and M. Sigrist, *Phys. Rev. B* **74**, 220506(R) (2006).

⁶Z. Hiroi, S. Yonezawa, Y. Nagao, and J. Yamaura, *Phys. Rev. B* **76**, 014523 (2007).

⁷G. Schuck, S. M. Kazakov, K. Rogacki, N. D. Zhigadlo, and J. Karpinski, *Phys. Rev. B* **73**, 144506 (2006).

⁸E. Ohmichi, T. Osada, S. Yonezawa, Y. Muraoka, and Z. Hiroi, *J. Phys. Soc. Jpn.* **75**, 045002 (2006).

⁹R. Galati, R. W. Hughes, C. S. Knee, P. F. Henry, and M. T.

Weller, *J. Mater. Chem.* **17**, 160 (2007).

¹⁰R. Khasanov, D. G. Eshchenko, J. Karpinski, S. M. Kazakov, N. D. Zhigadlo, R. Brütsch, D. Gavillet, D. Di Castro, A. Shengelaya, F. La Mattina, A. Maisuradze, C. Baines, and H. Keller, *Phys. Rev. Lett.* **93**, 157004 (2004).

¹¹R. Khasanov, D. G. Eshchenko, D. Di Castro, A. Shengelaya, F. La Mattina, A. Maisuradze, C. Baines, H. Luetkens, J. Karpinski, S. M. Kazakov, and H. Keller, *Phys. Rev. B* **72**, 104504 (2005).

¹²K. Magishi, J. L. Gavilano, B. Pedrini, J. Hinderer, M. Weller, H. R. Ott, S. M. Kazakov, and J. Karpinski, *Phys. Rev. B* **71**, 024524 (2005).

¹³M. Brühwiler, S. M. Kazakov, J. Karpinski, and B. Batlogg, *Phys. Rev. B* **71**, 214517 (2005).

¹⁴S. Yonezawa, Y. Muraoka, Y. Matsushita, and Z. Hiroi, *J. Phys. Soc. Jpn.* **73**, 819 (2004).

¹⁵Z. Hiroi, S. Yonezawa, T. Muramatsu, J. Yamaura, and Y. Muraoka, *J. Phys. Soc. Jpn.* **74**, 1255 (2005).

- ¹⁶S. Manalo, H. Michor, G. Hilscher, M. Brühwiler, and B. Batlogg, *Phys. Rev. B* **73**, 224520 (2006).
- ¹⁷S. M. Kazakov, N. D. Zhigadlo, M. Brühwiler, B. Batlogg, and J. Karpinski, *Supercond. Sci. Technol.* **17**, 1169 (2004).
- ¹⁸M. Brühwiler, S. M. Kazakov, N. D. Zhigadlo, J. Karpinski, and B. Batlogg, *Phys. Rev. B* **70**, 020503(R) (2004).
- ¹⁹Z. Hiroi, J. Yamaura, S. Yonezawa, and H. Harima, *Physica C* **460-462**, 20 (2007).
- ²⁰M. T. Weller, R. H. Hughes, J. Rooke, C. S. Knee, and J. Reading, *Dalton Trans.* **71**, 3032 (2004).
- ²¹J. Yamaura, S. Yonezawa, Y. Muraoka, and Z. Hiroi, *J. Solid State Chem.* **179**, 336 (2006).
- ²²M. Yoshida, K. Arai, R. Kaido, M. Takigawa, S. Yonezawa, Y. Muraoka, and Z. Hiroi, *Phys. Rev. Lett.* **98**, 197002 (2007).
- ²³SMART (Version 5.62), SAINT (Version 6.02), and SADABS (Version 2.03), Bruker AXS Inc., Madison, WI, 2002.
- ²⁴K. Kirschbaum, A. Martin, and A. A. Pinkerton, *J. Appl. Crystallogr.* **30**, 514 (1997).
- ²⁵G. M. Sheldrick, *SHELX97* (includes *SHELXS97* and *SHELXL97*), programs for crystal structure analysis (Release 97-2), Institut für Anorganische Chemie der Universität, Tammanstrasse 4, D-3400 Göttingen, Germany, 1998.
- ²⁶L. J. Farrugia, *J. Appl. Crystallogr.* **32**, 837 (1999).
- ²⁷T. P. Orlando, E. J. McNiff, S. Foner, and M. R. Beasley, *Phys. Rev. B* **19**, 4545 (1979).
- ²⁸A. M. Clogston, *Phys. Rev. Lett.* **9**, 266 (1962).
- ²⁹K. Maki, *Physica (Amsterdam)* **1**, 127 (1964).
- ³⁰N. R. Werthamer, E. Helfand, and P. C. Hohenberg, *Phys. Rev.* **147**, 295 (1966).
- ³¹V. G. Kogan, R. Prozorov, S. L. Bud'ko, P. C. Canfield, J. R. Thompson, J. Karpinski, N. D. Zhigadlo, and P. Miranović, *Phys. Rev. B* **74**, 184521 (2006).
- ³²Z. D. Hao, J. R. Clem, M. W. McElfresh, L. Civale, A. P. Malozemoff, and F. Holtzberg, *Phys. Rev. B* **43**, 2844 (1991).
- ³³M. Eisterer, M. Zehetmayer, H. W. Weber, and J. Karpinski, *Phys. Rev. B* **72**, 134525 (2005).
- ³⁴M. Karmakar and B. Dey, *Phys. Rev. B* **74**, 172508 (2006).
- ³⁵E. H. Brandt, *Phys. Rev. B* **68**, 054506 (2003).
- ³⁶I. L. Landau and H. Keller, *Physica C* **458**, 38 (2007).
- ³⁷E. H. Brandt, *Phys. Rev. Lett.* **78**, 2208 (1997).
- ³⁸A. M. Toxen, *Phys. Rev. Lett.* **15**, 462 (1965).
- ³⁹F. Marsiglio, J. M. Coombes, and J. P. Carbotte, *Phys. Rev. B* **35**, 3219 (1987).
- ⁴⁰J. Kuneš, T. Jeong, and W. E. Pickett, *Phys. Rev. B* **70**, 174510 (2004).
- ⁴¹M. Yoshida, K. Arai, R. Kaido, M. Takigawa, S. Yonezawa, Y. Muraoka, and Z. Hiroi, *J. Magn. Magn. Mater.* **310**, 698 (2007).
- ⁴²J. Schoenes, A.-M. Racu, K. Doll, Z. Bukowski, and J. Karpinski (unpublished).
- ⁴³M. Renninger, *Z. Phys.* **8**, 141 (1937).